8-12-2013

The Statistical Mapping of Magnetosheath Plasma Properties Based on THEMIS Measurements in the Magnetosheath Interplanetary Medium Reference Frame

A. P. Dimmock
Embry-Riddle Aeronautical University

K. Nykyri
Embry-Riddle Aeronautical University, nykyrik@erau.edu

JOURNAL OF GEOPHYSICAL RESEARCH: SPACE PHYSICS, VOL. 118, 4963–4976, doi:10.1002/jgra.50465, 2013

The statistical mapping of magnetosheath plasma properties based on THEMIS measurements in the magnetosheath interplanetary medium reference frame

A. P. Dimmock[1] and K. Nykyri[1]

Received 18 March 2013; revised 27 May 2013; accepted 21 July 2013; published 12 August 2013.

[1] The magnetosheath operates as a natural filter between the solar wind and the magnetospheric plasma. As a result of this, the magnetosheath plays a crucial role in the plasma momentum and energy transport from the interplanetary medium into the magnetosphere. Statistical studies of the magnetosheath are difficult due to the dynamic nature of the terrestrial bow shock and the magnetopause. As a result of this, the spatial and temporal dependence of magnetosheath plasma properties under varying solar wind conditions is still not completely understood. We present a study of magnetosheath plasma properties using 5 years of THEMIS and OMNI data to produce statistical maps of fundamental magnetosheath plasma properties. The magnetosheath interplanetary medium reference frame is applied to present data in a normalized reference frame which accounts for both boundary and orbital motion. The statistical maps are compared with the MHD runs from the CCMC-BATS-R-US model which agree favorably. The results are also used to investigate the presence of any magnetosheath plasma parameter asymmetries and their possible causes.

Citation: Dimmock, A. P., and K. Nykyri (2013), The statistical mapping of magnetosheath plasma properties based on THEMIS measurements in the magnetosheath interplanetary medium reference frame, *J. Geophys. Res. Space Physics*, *118*, 4963–4976, doi:10.1002/jgra.50465.

1. Introduction

[2] When the supersonic solar wind encounters the terrestrial magnetosphere (MSP) the forced rapid deceleration to subsonic velocities forms a standing shock wave upstream of the Earth. The region immediately behind the bow shock (BS) is occupied by the shocked, slower, hotter, and more turbulent plasma known as the magnetosheath (MS). The MS extends to the magnetopause (MP) which marks the boundary separating the MS and the magnetospheric plasma. As a result of this, the MS can be considered as a natural filter between the interplanetary and magnetospheric plasma. This "interface" therefore plays a fundamental role in the transport of SW plasma into the magnetosphere.

[3] The main process which occurs at the bow shock front is the redistribution of the upstream kinetic energy into other degrees of freedom [*Sagdeev*, 1966; *Sagdeev and Galeev*, 1969; *Papadopoulos*, 1985]. It has been demonstrated that the nature of these processes is highly sensitive to shock parameters such as the angle between the shock normal and the upstream magnetic field (Θ_{bn}), Mach number (M_a), cross-shock potential [*Dimmock et al.*, 2012], and the spatial scales within the shock transition (e.g., foot, ramp, and overshoot) [*Balikhin et al.*, 1995; *Newbury and Russell*, 1996; *Hobara et al.*, 2010]. Therefore, it is expected that MS plasma properties are delicately coupled with bow shock parameters and the induced particle interactions which take place at the shock front. Having said that, the highly nonlinear and complex nature of these processes means that uncovering the true extent of this effect is no trivial task. For that reason, it is not surprising that a complete understanding of how the SW plasma properties impact the MS plasma does not currently exist.

[4] Despite the substantial impact that the MS has on the magnetospheric system, there are surprisingly few large scale statistical studies devoted to MS plasma properties. One possible reason for this is the necessity for both in situ and thorough measurements performed over such a vast region. Furthermore, the orbital bias and configuration of spacecraft have to be suitable for such studies. It has been suggested that data sets originating from multiple missions could be combined to overcome the lack of data. However, the contrast in instrument design and calibration makes the direct comparison of these measurements complicated and questionable. In spite of this, the dynamic nature of the BS and the MP are arguably the main obstacle that impedes MS study. The shape and location of these boundaries respond directly to variations in the SW, which can make accurate identification of the MS a complicated task. With respect to case studies, the significance of this problem is reduced. On

[1]Department of Physical Sciences, Embry-Riddle Aeronautical University, Daytona Beach, Florida, USA.

Corresponding author: A. P. Dimmock, Department of Physical Sciences, Embry-Riddle Aeronautical University, Daytona Beach, FL, USA. (dimmocka@erau.edu)

2169-9380/13/10.1002/jgra.50465

the other hand, the continuous motion of the MP and BS means that direct comparison of MS properties under different SW conditions can be unreliable. For that reason, large scale statistical studies of MS plasma properties are complicated since results presented in frames such at the Geocentric Solar Ecliptic (GSE) or Geocentric Solar Magnetospheric (GSM) do not inherently account for any motion of the MS boundaries. To further complicate matters, the orbital motion of the Earth must also be accounted for. In addition to this, it has been suggested [*Peredo et al.*, 1995; *Verigin et al.*, 2001] that the varying orientation of the interplanetary magnetic field (IMF) causes a dawn-dusk asymmetry in the BS location, which results in an asymmetrical MS thickness that increases tailward. Magnetohydrodynamic (MHD) simulations are free from these physical restrictions and can go to considerable lengths to understanding and predicting the behavior of MS plasma properties. However, their lack of kinetic physics provides only a limited view. Statistical studies based on experimental data are useful as they include both MHD and kinetic physics but are plagued by both the aforementioned complications and the biased spacecraft configuration, which are often directed toward the study of different regions or plasma processes.

[5] Case studies such as that performed by *Petrinec et al.* [1997] use observational data to determine the boundary crossing locations. In this particular work, the authors found that for the chosen cases, the MS flow speeds were largest when the angle between the local magnetic field and velocity vectors were more perpendicular. Interestingly, this property was not observed close to the BS. For the examples studied, the MS flow speeds did not exceed that of the SW measured at the time. In this particular study, only several crossings were analyzed; therefore, observational data was an ideal method to identify boundary locations. In contrast, studies of a statistical nature are composed of extremely large data sets (several years), and therefore, a more automated and practical approach has to be taken.

[6] *Němeček et al.* [2000] performed a statistical study of MS ion flux where INTERBALL-1 provided the MS measurements, and WIND behaved as a solar wind monitor. The authors used the *Shue et al.* [1998] MP and *Formisano* [1979] BS models to determine both boundary locations based on the SW conditions provided by WIND. These were then used to transform each spacecraft position from the GSE frame into a new aberrated frame which was normalized across the MS thickness. They compared model predicted and measured values of ion fluxes at each point and found that observations were smaller than or equal to the model output. It was also suggested that experimental data saturated when moving from the middle of the MS toward the BS, whereas model predictions continued to rise. It was implied that the IMF B_z component controls dayside MP ion flux but not the nightside. Other statistical studies of MS plasma properties such as those by *Paularena et al.* [2001], *Longmore et al.* [2005], *Verigin et al.* [2006], & *Lavraud et al.* [2013] have adopted a similar approach by applying the magnetosheath interplanetary medium (MIPM) reference frame [*Bieber and Stone*, 1979]. The boundary locations are identified using predetermined models which allow the calculation of a normalized spacecraft position vector in a new aberrated frame based on the SW IMF and velocity vectors. Once all transformations are complete, MS data can be analyzed as if the MP and BS are stationary. *Paularena et al.* [2001] used IMP 8, ISEE, and WIND data to investigate the plasma density in the MS dawn and dusk flanks. The result from this study showed a plasma density dawn-dusk asymmetry which favors the dawnside. Interestingly, this asymmetry was more pronounced during the solar maximum cycle between 1978 and 1980 than the solar minimum period of 1994–1997. *Longmore et al.* [2005] performed a study of MS plasma properties using Cluster data, and the results from this work also suggests stronger dawn densities but also higher flow velocities on the dusk flanks. The authors also imply a tendency for higher flow speeds and values of density at the BS which decreases with proximity to the MP. A recent study performed by *Walsh et al.* [2012] using Time History of Events and Macroscale Interactions during Substorms (THEMIS) data also supports the results from *Paularena et al.* [2001]. In addition to this, their results also reported larger magnetic field and velocity magnitudes on the dusk flank whereas, on the contrary, ions appear to be hotter on the dawn flank. Evidence of dawn ion temperature asymmetry was also suggested by *Wing et al.* [2005] in which cold component ions were 30%–40% hotter on the dawnside of the magnetospheric plasma sheet. Although the IMF has direct control over the quasi-parallel ($\Theta_{\parallel}$) and quasi-perpendicular ($\Theta_{\perp}$) regions of the BS and asymmetries have been observed during these regimes, *Longmore et al.* [2005] observed no dependence of these asymmetries on the IMF orientation. An explanation of this could be due to the orbital bias of the Cluster mission which favors a polar orbit, but it is also likely that other physical processes have a pivotal role in the presence of these asymmetries. In a study by *Lavraud et al.* [2007], strong plasma bulk flows were observed in the MS, which exceeded present SW conditions. These flows were not caused by reconnection but possibly arose due to a magnetic "sling-shot" effect originating from enhanced magnetic forces during low β and low Alfvén Mach number SW conditions. A recent study by *Hietala et al.* [2012] has shown that supersonic flows can also be present downstream of the bow shock. The presence of such flows was attributed to the rippling behavior of the shock front.

[7] The THEMIS mission was launched in 2007 with the scientific objective of studying the onset of magnetospheric substorms. The nature of this task meant that the THEMIS probes were placed in varying orbits with apogees ranging from around 10 Re to around 30 Re translating to orbital period of 1 to 4 days [*Frey et al.*, 2008]. A useful attribute from this configuration is the availability of measurements in the far tailward direction, which are not available from other missions. Although this mission was completed in 2010, the probes are still operational and continue to transmit data which culminates in an extensive 5 year database containing in situ observations of the magnetosphere and the surrounding plasma environment. The abundance of measurements, comprehensive coverage, and favorable orbital bias therefore make the THEMIS database well suited to statistical studies of the MS. The following manuscript presents a statistical study of MS plasma properties using THEMIS as a source for MS measurements in combination with OMNI data sets acting as an upstream SW monitor. We apply the MIPM reference frame to bin experimental data so that boundaries are considered

stationary and thus allows the comparison of MS observations collected under different SW conditions. Statistical data sets are compiled from MS observations spanning a 5 year (2007–2013) period, which are then binned into a square grid-space (0.5 Re × 0.5 Re) to produce statistical maps of magnetic field, plasma velocity, and ion density. The experimental results will be compared with the output from MHD simulations and any discrepancies will be discussed.

[8] The following manuscript will be structured as follows. Section 2 will introduce the methodology that is used to convert data in the GSE frame to the MIPM frame. Section 3 will provide a description of the experimental and theoretical resources required to complete this work. Section 4 will discuss the technical aspect of this study in terms of the data processing required to obtain our statistical data. This section will also cover the selection criteria employed when selecting appropriate MS measurements. Finally, the results will be presented and compared with the output from the CCMC BATS-R-US MHD simulations. Discussion of the results in context with the scientific implications will follow and the final conclusions will be drawn.

2. Conversion From the GSE to the MIPM Reference Frame

[9] The following section describes the methodology applied to transform the location of each THEMIS probe initially in the GSE frame, to the required MIPM reference frame. The MIPM frame is an extension of the geocentric interplanetary medium (GIPM) frame [see *Verigin et al.*, 2006, and references therein] which has an x axis ($\mathbf{e}_x$) antiparallel to the upstream solar wind.

$$\mathbf{e_x} = \frac{[-V_x, -V_y - V_e, -V_z]}{\sqrt{V_x{}^2 + (V_y + V_e)^2 + V_z{}^2}} \tag{1}$$

$\mathbf{e}_x$ removes the Earth's orbital velocity (V_e) and thus accounts for the orbital motion. The y axis ($\mathbf{e}_y$) is primarily dictated by the IMF configuration which accounts for the BS asymmetry present in the terminator plane.

$$\mathbf{e_y} = \begin{cases} -\mathbf{B} + (\mathbf{B}\cdot\mathbf{e_x})\mathbf{e_x}/|\mathbf{B} - (\mathbf{B}\cdot\mathbf{e_x})\mathbf{e_x}|, & \text{if}(\mathbf{B}\cdot\mathbf{e_x}) > 0, \\ +\mathbf{B} - (\mathbf{B}\cdot\mathbf{e_x})\mathbf{e_x}/|\mathbf{B} - (\mathbf{B}\cdot\mathbf{e_x})\mathbf{e_x}|, & \text{if}(\mathbf{B}\cdot\mathbf{e_x}) < 0, \end{cases} \tag{2}$$

The three-axis set is then finally completed by performing the cross product between $\mathbf{e}_x$ and $\mathbf{e}_y$

$$\mathbf{e_z} = \mathbf{e_x} \times \mathbf{e_y} \tag{3}$$

In equations (1) and (2), the variables **V** and **B** represent the SW velocity and magnetic field strength respectively measured in the GSE frame. For the majority of cases (PS IMF), the GIPM frame differs only slightly from the GSE frame (few degrees); however, the main discrepancy is the change in the orientation of $\mathbf{e}_y$ and $\mathbf{e}_z$ when the IMF configuration switches from PS to OPS.

[10] The MIPM reference frame consists of a zenith angle (θ), clock angle (ϕ), and a radial fraction distance $F_{\text{mipm}}(\theta, \phi)$ which is a function of the latter two angles (see Figure 1). The angles θ and ϕ are defined by the geometry between the GSE position vector **R**, and the GIPM $e_{x,y,z}$ axes, i.e.,

$$\begin{aligned} \theta &= \arccos((\mathbf{R}\cdot\mathbf{e_x})/|\mathbf{R}|) \\ \phi &= \arctan((\mathbf{R}\cdot\mathbf{e_z})/(\mathbf{R}\cdot\mathbf{e_y})) \end{aligned} \tag{4}$$

In practice the full range ($0 \rightarrow 2\pi$) of θ and ϕ is obtained using the perspective from e_z and e_x respectively. The fractional distance (F_{mipm}) is a function of both θ and ϕ, which can be described as a normalized distance across the model MS. The calculation of F_{mipm} therefore requires knowledge of the geocentric distance from the probe location, to the BS (r_{bs}) and MP (r_{mp}). First, r_{bs} is estimated from the BS model by *Verigin et al.* [2001].

$$\begin{aligned} r_{\text{BS}}\cos(\theta) &= r_0 + \Delta + \chi R_s(M_{\text{as}}{}^2 - 1) \\ &\quad -0.5(1-\chi)r_{\text{BS}}\sin(\theta)\sqrt{M_{\text{as}}{}^2 - 1} \\ &\quad -\chi R_s(M_{\text{as}}{}^2 - 1)K \end{aligned} \tag{5}$$

and second, r_{mp} is calculated from the MP model by *Shue et al.* [1998].

$$r_{\text{MP}} = r_0\left(\frac{2}{1+\cos(\theta)}\right)^{\alpha} \tag{6}$$

To maintain continuity, we refer you to Appendix A for a full description of the variables present in equations (5) and (6). It is worth noting that the solution of equation (5) requires downstream measurements directly behind the BS nose. Although various spacecraft inside the MS could be used to obtain this information, the occasions where spacecraft would be located at appropriate locations are uncommon, thus making statistical studies very difficult. Therefore, to obtain an estimate of the upstream/downstream density ratio (ϵ), we use the Rankine-Hugoniot relations [*Verigin et al.*, 2001] assuming a ratio of specific heats value of $\lambda = 5/3$.

[11] The fractional distance (F_{mipm}) is therefore the normalized distance at **R**, measured between r_{mp} and r_{bs}, i.e.,

$$F_{\text{mipm}} = \frac{|\mathbf{R}| - r_{\text{MP}}}{r_{\text{BS}} - r_{\text{MP}}} \tag{7}$$

F_{mipm} can therefore be broken down as follows

$$F_{\text{mipm}} = \begin{cases} (0 \rightarrow 1), & \text{MS}, \\ (<0), & \text{MSP}, \\ (>1), & \text{SW}, \\ (1), & \text{BS}, \\ (0), & \text{MP}, \end{cases} \tag{8}$$

F_{mipm} serves two purposes as it can be used, first, to determine what region the probe occupies and, second, when $0 \leq F_{\text{mipm}} \leq 1$ the magnitude of F_{mipms} is a direct indication of the distance across the MS. Each data point undergoes the transformation from the GSE frame into MIPM frame, and the details of this process will be discussed in the proceeding sections.

[12] The MIPM reference frame differs significantly in comparison with the GSE frame. Crucially, in the MIPM frame, the IMF orientation plays a crucial role in the placement of statistical data points. Principally, data points are organized with respect to the shock geometry resulting from the IMF configuration. For example, under a parker-spiral (PS) IMF, the points conform to the typical GSE dawn ($\Theta_{\parallel}$)-dusk($\Theta_{\perp}$) configuration. However, under an ortho-Parker

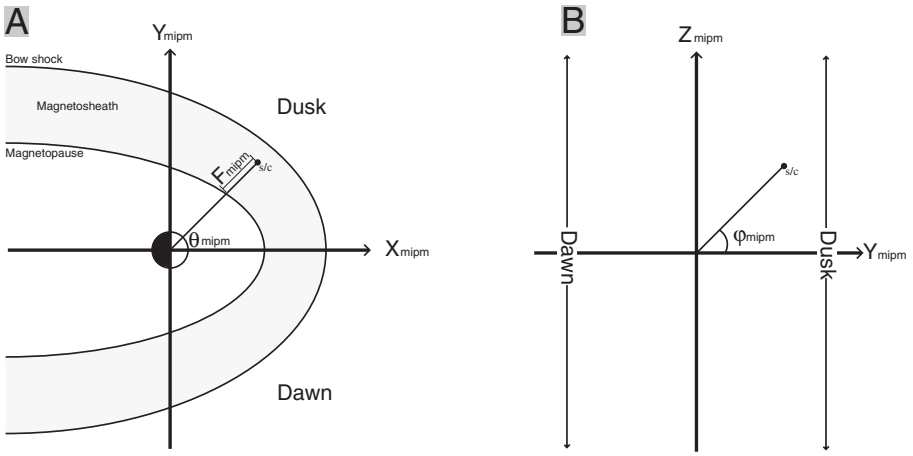

Figure 1. A single spacecraft location represented in the MIPM frame. (left) The zenith angle in an XY plane. (right) The clock angle in the YZ plane.

spiral (OPS) IMF, the points are then anticorrelated with the GSE frame and are placed in a dawn($\Theta_\perp$)-dusk($\Theta_\parallel$) arrangement. Therefore, the dawn-dusk terminology will be replaced with $\Theta_\perp$ and $\Theta_\parallel$ where $\Theta_\perp \rightarrow Y_{mipm} > 0$ and $\Theta_\parallel \rightarrow Y_{mipm} < 0$. Owing to the fundamental role that the BS plays on the formation of the MS plasma, presenting data with respect to shock geometry is quite intuitive. On a statistical basis, it prevents the overlap of plasma properties which have been transmitted under different shock configurations. This attribute will help to investigate the dependence of MS plasma properties on shock geometry dictated by the IMF orientation.

3. Data Sets and Instrumentation

[13] All of the measurements inside the MS originated from the comprehensive array of instrumentation onboard each of the five THEMIS probes [*Angelopoulos*, 2008]. This study utilizes the complete available period which spans a time interval between 2007 and 2013. Estimates of the magnetic field in the MS were provided by the fluxgate magnetometer (FGM) instrument [*Auster et al.*, 2008] onboard each spacecraft. Each FGM instrument provides full three-axis magnetic field measurements at a maximum cadence 64 vec/s with the capability to detect perturbations of 0.01 nT. Such a high resolution and sensitivity is surplus to our requirement and for that reason, spin resolution ($\approx$ 3 s) FGM data are used. The remaining plasma properties of velocity ($\mathbf{V}^{ms}$), density (N^{ms}) and pressure (P^{ms}) are all acquired from the THEMIS plasma moment files which are calculated onboard by the moments for Electrostatic Analyzer (ESA) instrument [*McFadden et al.*, 2008]. The associated derived quantities such as plasma β are also calculated from these data sets.

[14] All SW measurements are taken from the OMNI (http://omniweb.gsfc.nasa.gov) database which is constructed from both magnetic field and plasma measurements recorded by the Advanced Composition Explorer (ACE) [*Stone et al.*, 1998], Wind [*Acuña et al.*, 1995], Interplanetary Monitoring Platform-8 (IMP 8) and Geotail missions [*King and Papitashvili*, 2005]. The purpose of this database is to provide continuous estimates of magnetic field and plasma moments at the bow shock nose ($\approx$ 15 Re). These measurements are not in-situ but are propagated from the upstream spacecraft positions to the BS nose using the BS model by *Farris and Russell* [1994]. In the present study these measurements are required for two purposes, firstly in the process when converting from the GSE frame to the MIPM frame, and secondly as a method to bin MS data under different SW conditions (eg. IMF orientation). These data are available in low resolution of 1 hr, 1 day and 27 days which cover the period from 1963 to the present day. Higher resolution data files of 1 and 5 minute vec/sec are also available which start from the later date of 1995. All of the OMNI data gathered for this study were taken from the monthly 1 minute data files over the corresponding THEMIS duration.

[15] All the simulated results presented later in this manuscript were produced by the BATS-R-US [*Tóth et al.*, 2005] MHD model, which is available through the Community Coordinated Modeling Centre (CCMC) (http://ccmc.gsfc.nasa.gov).

4. Data Processing and Selection Criteria

[16] For each MS data point there has to be corresponding SW conditions so that an accurate position of the MP and BS can be provided. Because the boundary locations are used directly in the transformation from the GSE to the MIPM frame, any error induced in their estimation will be transported directly to the placement of points in the statistical data set. The main concern here, is the spatial and temporal "lag/offset," which takes place between the BS nose and the physical probe location. Another possible introduction of error could arise from transient perturbations in the SW, which would result in an inaccurate estimate of the ambient SW conditions. To overcome these difficulties, we select a 20 min window ($\pm$ 10 min) surrounding each 1 min OMNI measurement. To provide an estimate of the SW conditions, each plasma property is averaged within each window. If there is less than 50% of data available within any given window, this period is flagged and excluded from the following statistical data set.

[17] For each averaged OMNI window, the corresponding THEMIS data is identified. THEMIS state data files are

used to obtain the location of each THEMIS probe in the GSE frame (**R**). At each available **R**, the MS boundary positions are calculated from equations (5) and (6) and then converted to the MIPM reference frame using equations (4) and (7). These calculations are based on the 20 min averaged OMNI data and are only included if the above criteria are met. Following this, to "smooth" the MS measurements, a 3 min ($\pm$ 90 s) windowed average is also applied for each plasma property corresponding to each THEMIS position. The criterion demanding at least 50% window coverage is still applied.

[18] In addition to adequate coverage, the fluctuation of each MS parameter within each window is also a concern. During periods where a large variation of any parameter takes place, then it would be desirable to eliminate these cases from our results. However, each plasma property is measured on a different scale, which means that measuring the fluctuation/turbulence is subjective to the property which is being observed. To facilitate the direct comparison of various plasma properties, the data has to be normalized so units or scale are no longer a concern. Thus, the z score of each data point within all windows is evaluated. The Z score is a dimensionless quantity which represents any sample in measures of standard deviations (σ) from the mean (μ) derived from the larger population, i.e.,

$$Z_w = \frac{X_w - \mu_p}{\sigma_p} \tag{9}$$

The subscripts w and p refer to the window and larger population, respectively. The larger population is assumed to be the 24 h data set that the window is comprised. This process allows comparison of different plasma observations by normalizing each data window. The standard deviation of each z-window must conform to $Z_{\mathrm{win}} < 1$ to be within acceptable limits. However, if $Z_{win} > 1$,then the data window is flagged and therefore omitted.

[19] The MS data is then extracted based on the magnitude of F_{mipm} (i.e., $0 \leq F_{\mathrm{mipm}} \leq 1.$). All individual probe databases are then merged to form the complete statistical database. The conversation from the GSE to MIPM frame is dependent on the accuracy of the BS and MP models, which are evaluated for each data point. However, no model is 100% accurate, and it is inevitable that the misidentification of SW and MSP points will take place. Arguably, the BS can be considered a more dynamic boundary than the MP as its evolution is much more vulnerable to changes in upstream plasma conditions. As a result of this, we include check conditions which attempt to eliminate SW data points that were misidentified in earlier stages. We rely on the velocity ratio ($V_{d/s} = V^{\mathrm{MS}}/V^{\mathrm{SW}}$) measured upstream and downstream of the terrestrial bow shock. In our results, we do not include data points where the MS velocity exceeds that of the SW velocity. It has to be mentioned that previous studies have shown that it is possible for supersonic flows to exist due to processes such as rippling of the shock surface [see *Hietala et al.*, 2012]. In addition to this, *Lavraud et al.* [2007] reported cases where this condition can be violated during conditions such as high SW velocities (1000+ km/s in the MS, while only 650 km/s in the SW). However, the focus of this work is directed toward mapping the global MS profile, and therefore, the occurrence of these points should be less in comparison to standard SW conditions and should not impact our results.

[20] For each MS measurement, there is a corresponding estimate of the instantaneous SW conditions. The availability of these measurements allows the extraction of MS measurements for various SW conditions such as IMF orientation, density and velocity, etc. It is also possible to combine multiple upstream conditions to create custom statistical data. However, as the parameterization becomes more stringent, then subsequently less amount of data becomes available. Therefore, a "trade-off" arises between the amount of prefiltering which can be performed and is controlled by the amount of statistical data available. It is worth noting that a useful property of this methodology is the ability to reverse the process and isolate specific SW conditions by extracting specific MS plasma properties. Following the compilation of the statistical data described in the preceding text, the full database is then filtered with respect to various SW conditions to form multiple statistical databases unique to various upstream SW conditions. These data sets can then be processed individually to produce experimental maps of the MS representing various SW plasma properties.

4.1. Binning of Experimental Data

[21] At this point, the MIPM data points are represented by θ_{mipm}, ϕ_{mipm}, and $\mathrm{F_{mipm}}$, which is not ideally suited for binning into a cartesian grid space. Therefore, they are converted to a cartesian coordinate system based on averaged upstream conditions derived from the distributions displayed in Figure 2. However, initially, $\mathrm{F_{mipm}}$ has to be denormalized and expressed as a physical quantity $\mathrm{R_{mipm}}$. The following expression describe this conversion:

$$R_{\mathrm{mipm}} = R_{\mathrm{mp}}{}^{*} + [F_{\mathrm{mipm}}(R_{\mathrm{bs}}{}^{*} - R_{\mathrm{mp}}{}^{*})] \tag{10}$$

where the superscript asterisk (*) denotes that these values are calculated using average SW conditions. This conversion is purely used as a means to bin the statistical data sets. Although average SW conditions are used, the boundary and orbital motion have already been accounted for in the initial frame conversion in equations (4) and (7). A MIPM gridspace is then constructed for the MIPM XY plane between $-50 \rightarrow 20$ Re along the $\mathrm{X_{mipm}}$ direction, and $\pm$ 50 Re along the $\mathrm{Y_{mipm}}$ axis. Although the grid dimensions can be varied, this current study uses a grid dimension of 0.5 Re $\times$ 0.5 Re. This was specified as it provided the best overall trade off between data availability (within each grid) and resolution for the maps. Increasing the resolution (decreasing grid dimension) also has a significant effect on the computational expense required to process each statistical database. The binning process assigns each individual data point to a corresponding bin. In the rare event that a point falls on the boundary between multiple grids, then this point is included in all bins to which the boundary is shared. Once that all points have been processed, each individual grid is averaged (for all plasma properties) to provide a weight. The grid space is then plotted based on the shading of each grid where the color reflects the bin weight.

5. Results

[22] The preceding text has outlined the methodology used to complete this study. The current section will discuss

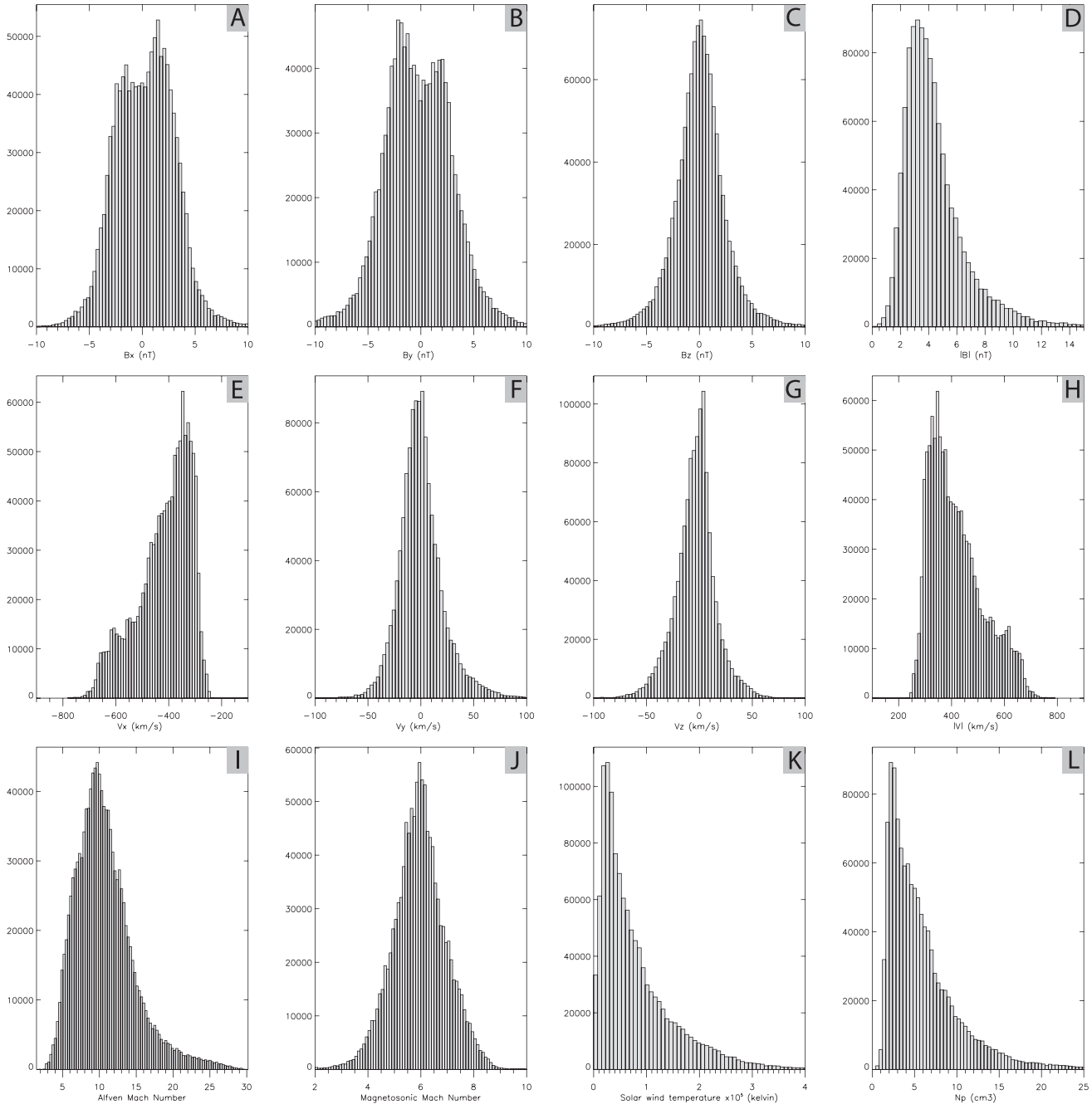

Figure 2. Histograms showing the distribution of SW conditions compiled from OMNI data corresponding to the time interval when at least one of the THEMIS probes were in the MS.

the results which were obtained from the application of these processing techniques to over 5 years of THEMIS measurements. Statistical maps are presented for plasma velocity, magnetic field, and density, and in addition to this, simulated MHD results are also provided for the same quantities.

5.1. Solar Wind Data

[23] Figure 2 shows the distribution of SW plasma properties for the full statistical data set (no prefiltering) recorded when the five THEMIS probes traversed the MS. The histograms from Figures 2a and 2b show the distribution of the x and y components of the IMF vectors compiled from the OMNI database. Both of the distributions differ by a distinguishable "bump" located at +2.5 nT and –2.5 nT for B_x and B_y, respectively. The significant result from these statistics is that they provide evidence that the IMF is predominantly in the PS orientation. The shift from a PS to a OPS IMF orientation is of primary concern as it directly controls allocation of the quasi-perpendicular and quasi-parallel regions of the BS. Therefore, statistically, in the GSE frame $Y_{GSE} > 0$ represents a quasi-perpendicular BS geometry and $Y_{GSE} < 0$ a quasi-parallel. As a result, the majority of downstream plasma has been processed under this configuration. In contrast, the distribution of B_z shown in Figure 2c appears to be

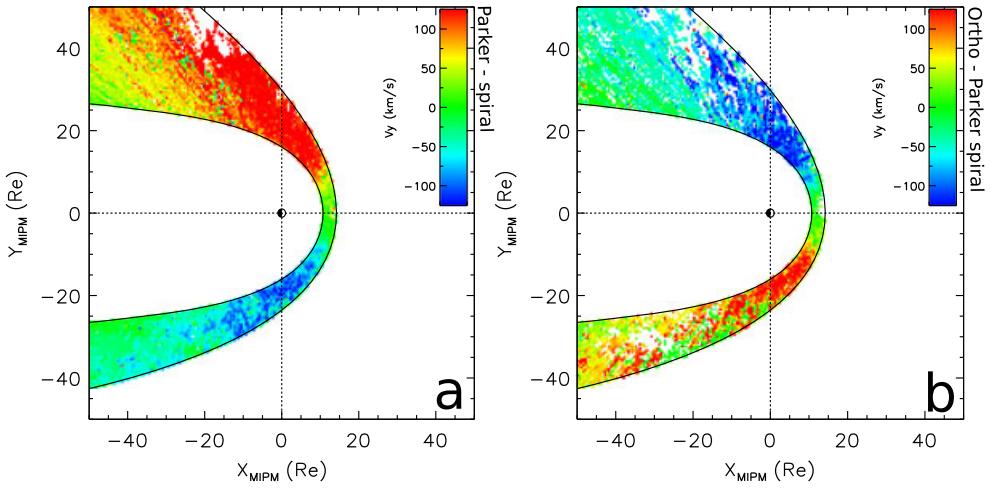

Figure 3. Statistical maps compiled for the y component of plasma velocity for IMF orientations of (a) PS and (b) OPS, respectively.

well characterized by a standard normal distribution with no distinct features. This suggests the majority of IMF vectors compiled for this study consist of small ($\pm$ 1 nT) to negligible B_z components. The significance of B_z can be understood from equations (2) and (4), because any significant increase in B_z will rotate a MIPM point out of the XY plane. The small concentration of B_z (–2.5 $\rightarrow$ 2.5) suggests this should not have a notable effect on the statistical maps.

[24] Figure 2h shows the distribution of the magnitude of the SW plasma velocity vectors. The histogram is clearly centered around 350 km/s, which is representative of typical SW conditions. There are speeds which are in excess of 700 km/s, but their occurrence is significantly reduced in comparison to lower velocities. Nevertheless, these high velocities have been previously reported due to the presence of CMEs and similar phenomena. The histogram which shows the distribution of Alfvén Mach number (Figure 2i) suggests that the mean value is approximately 10 and the vast majority of data falls in the range between 5 and 15. The magnetosonic Mach number is distributed around a mean value of 6 which can be seen from the histogram. Although the majority of magnetosonic Mach numbers are between 4 and 8, during extreme cases, they can exceed 9. The average SW ion temperature is approximately 3×10^5 K but ion temperatures can reach beyond 25×10^5 K in some cases. The SW proton density shown in Figure 2l suggests a distribution that is gathered around 2–3 cm^{-3}, and the majority of data varies between 2 and 10 cm^{-3}.

5.2. Magnetosheath Plasma Velocity

[25] Figure 3 represents the y component of plasma velocity in the MS during intervals where the IMF is PS and OPS. Figures 3a and 3b represent the statistical data binned only for PS and OPS IMF, respectively. In the GSE frame, the plasma flow along the GSE y direction is typically positive and negative on the dusk and dawn flanks, respectively. Notably, this feature is independent of the PS and OPS IMF orientation. This particular observation is very useful as it provides direct and graphical means of validating the placement of points in the MIPM frame. Under a PS IMF, the MIPM frame differs by only a few degrees to the GSE frame, but this cannot be said for the OPS case. The obvious exception is that whereas GSE points correspond directly to their spatial coordinates, the MIPM frame sorts data with respect to upstream IMF orientation and thus BS geometry. For example, under a typical PS IMF, the statistical results should coincide directly with the expected results. On the contrary, when the IMF is in an OPS configuration, then the BS geometry has changed and, therefore, we would expect the statistical maps to reflect this by placing positive flow velocities in the $Y_{mipm} < 0$ region and negative in the $Y_{mipm} > 0$ flank. The allocation of statistical data in the MIPM frame is clearly demonstrated by the differences between Figures 3a and 3b. In addition to this, both the experimental figures show that velocity at the BS nose is approximately zero, which then increases (in $\pm$ direction) downtail to around $\pm$150 km/s, which is typical of the MS profile and consisted of MHD simulations (not shown). The purpose of Figure 3 is to demonstrate the placement of points in the MIPM frame.

[26] The normalized magnitude of the MS plasma velocity is demonstrated by Figure 4. Figures 4a and 4b represent the statistical results for all available data whereas Figure 4d shows MS plasma velocity for a PS IMF obtained from the CCMC BAT-R-US MHD code. Figures 4a and 4b represent the mean and median of all points which fall into each 0.5 $\times$ 0.5 Re bin. Figure 4c, on the other hand, demonstrates the number density of data points collected within each bin (cc). Please note that the experimental values have been normalized by their simultaneous upstream velocities whereas the MHD result has not. The statistical plots conform with the expected MS velocity profile where slowest velocities are located at the BS nose and then increased tailward. The velocity also appears to decrease from the BS to the MP. Average velocities at the MP stagnation point are $\approx$ 0.15 however in close vicinity to the BS nose typical values peak around 0.25. When moving away from the BS nose into a thicker MS, these quantities increase to 0.5 ($X_{mipm} \approx 5$ Re) before reaching 0.7 at the dayside/nightside terminator. Further tailward, there is a notable increase from 0.7 to a region where quantities average 0.9. This acceleration is expected from simulated results which imply that the MS velocity

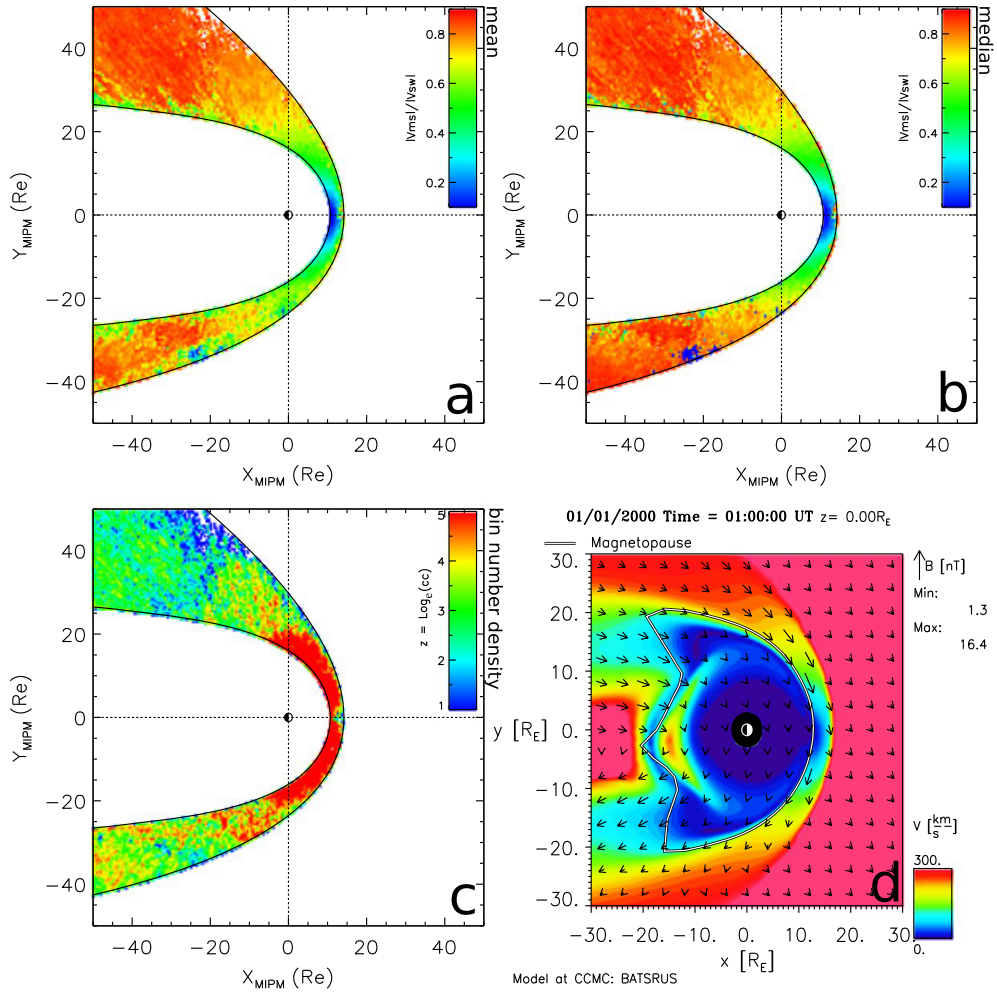

Figure 4. Statistical maps for normalized MS velocity magnitude for all experiment data using the (a) mean and (b) median averages of data, which falls into each 0.5 × 0.5 Re bin. (c) The count per bin (cc) and (d) the MHD simulated result for MS plasma velocity magnitude in km/s during a PS IMF orientation.

eventually "catches up" with the SW far enough downtail. The velocity profiles based on experimental data (Figures 4a and 4b) exhibit these described characteristics. Reference to Figures 4a and 4b suggests that the MS velocity is on average greater on the $\Theta_{\perp}$ flank. In the GSE frame, this would correspond to the dusk region of the MS for PS and dawn for OPS IMF. The velocity asymmetry does not appear to be present between the BS nose and the terminator but is particularly visible in the area encompassed between $-10 \leq X_{mipm} \leq 5$ Re. Far downtail (≈ -40 Re), the velocity profile on each side tends to unity and this asymmetry becomes even less apparent. There is a clear discrepancy between the data binned in the $\Theta_{\parallel}$ flank for the mean and median averages. The median bins appears to show slightly higher velocities than the mean values from around –10 Re tailward. Having said that, the velocity on the $\Theta_{\perp}$ flank is still higher than the $\Theta_{\parallel}$ flank in the region close to the terminator (–10 Re $\rightarrow$ 5 Re) and the same conclusion can be reached for either statistical plots. The small blue region in Figure 4b on the $\Theta_{\parallel}$ flank at –20 Re appears to be an artificial result and sensitive to the mean/median averages but does not interfere with our interpretation of this data. The most significant outcome from the median average is that this asymmetry appears to disappear tailward beyond –20 Re. Reference to Figures 4a and 4b implies that there is agreement showing that the observed velocity asymmetry is most prominent in the region close to the terminator. Reference to Figure 4c shows that around the region of interest, there is the most comprehensive data coverage with typically 30–50+ points contributing to each bin. In general, the dayside has the most extensive coverage which then decreases tailward.

5.3. Magnetosheath Ion Density

[27] Figure 5 represents the statistical and simulated results for plasma ion density. The arrangement of this figure is the same as Figure 4. Statistical data in Figures 5a and 5b have been normalized by their upstream values, whereas the simulated results in Figure 5d express the number density per cm^3. Results based on statistical and simulated data show a region of high density that extends between the BS nose and $X_{mipm} \approx -5$. During this region, the normalized and physical values are approximately 5 and 10, respectively. Around the day/night terminator, the region of high density diminishes, and typical normalized values are ≈ 2.5 and 7.5 in the simulated case. The density far downtail ($X_{mipm} < -30$) eventually matches the SW value in regions

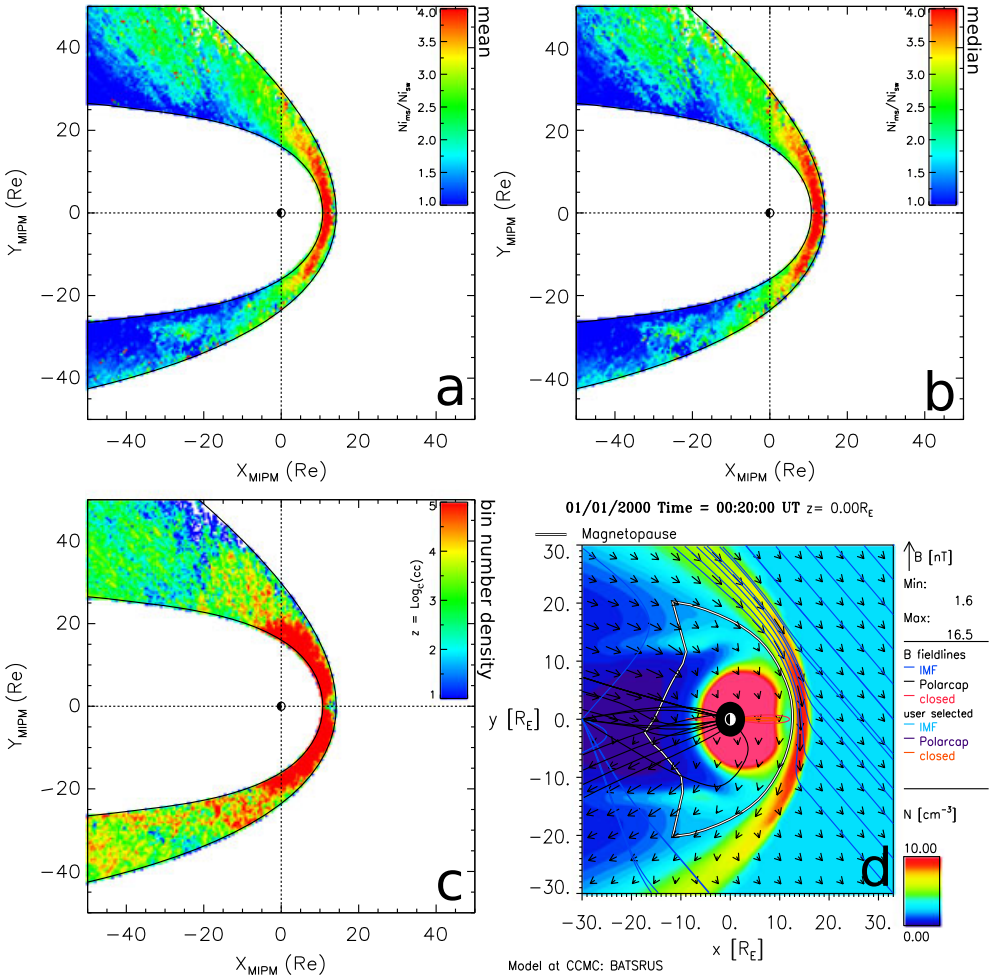

Figure 5. Statistical maps for normalized ion density for all experiment data using the (a) mean and (b) median averages of data, which falls into each 0.5 × 0.5 Re bin. (c) The count per bin (cc) and (d) the MHD simulated result for MS ion number density per cm^3 during a PS IMF orientation.

within relatively close proximity to the MP (≈ 5 Re) on both flanks. The MHD result shows a similar feature but suggests that a small asymmetry is present at the dawn flank ($Y_{gse} < 0$). In its present form, the statistical maps exhibit no tangible evidence of $\Theta_\perp - \Theta_\parallel$ asymmetry in either mean or median averaged statistical data. The data compiled only for the OPS IMF configuration (not shown) exhibit very similar features as mentioned above and also does not suggest any strong asymmetry about the X_{mipm} axis. The data coverage in Figures 5 and 4 are very similar, which suggests that the absence of any observed asymmetry should not be a consequence of data coverage. There are also negligible differences between the mean and median bin values in Figures 5a and 5b suggesting that this result is not the result of statistical averaging.

5.4. Magnetosheath Magnetic Field Strength

[28] Figure 6 shows the MS magnetic field strength with the same arrangement as Figures 3 and 4. Figures 6a and 6b represent the statistical mean and median averaged bins whereas Figure 6c shows the count per bin. Figure 6d represents the simulated result for a PS IMF. In the experimental case, the values have been normalized with respect to their upstream counterpart. The MHD run shows a region of enhanced magnetic field close to the MP and BS nose. This region is consistent with the build up of magnetic field typically associated with the MP stagnation point. Moreover, when moving from the MP toward the BS, there is a general decrease of magnetic field strength. In the region past the terminator downtail, this feature gets less obvious and forms a steady band of ≈ 8 nT on the $\Theta_\perp$ (GSE dusk) flank. There is a clear asymmetry in the MHD run which shows that magnetic field strength is clearly stronger on the dusk flank during PS IMF conditions and is clearly noticeable in the region between $0 \leq X_{mipm} \leq 5$ Re. Interestingly, for the simulated case during an OPS IMF (not shown), this asymmetry manifests on the opposite dawn flank. Therefore, in the simulated environment, MHD theory shows enhanced magnetic fields, which favor the region processed by the quasi-perpendicular shock. In comparison with the experimental results, there are remarkably similar features. The enhanced field close to the MP at the BS nose is clearly distinguishable. In Figure 6a, there is clearly a greater magnetic field strength on the $\Theta_\perp$ flank, which is most noticeable in the areas close to the terminator. Downtail and close to the MP, the magnetic field strength gradually decreases which is also suggested by the MHD result. Both mean and median averaged data sets exhibit the same general

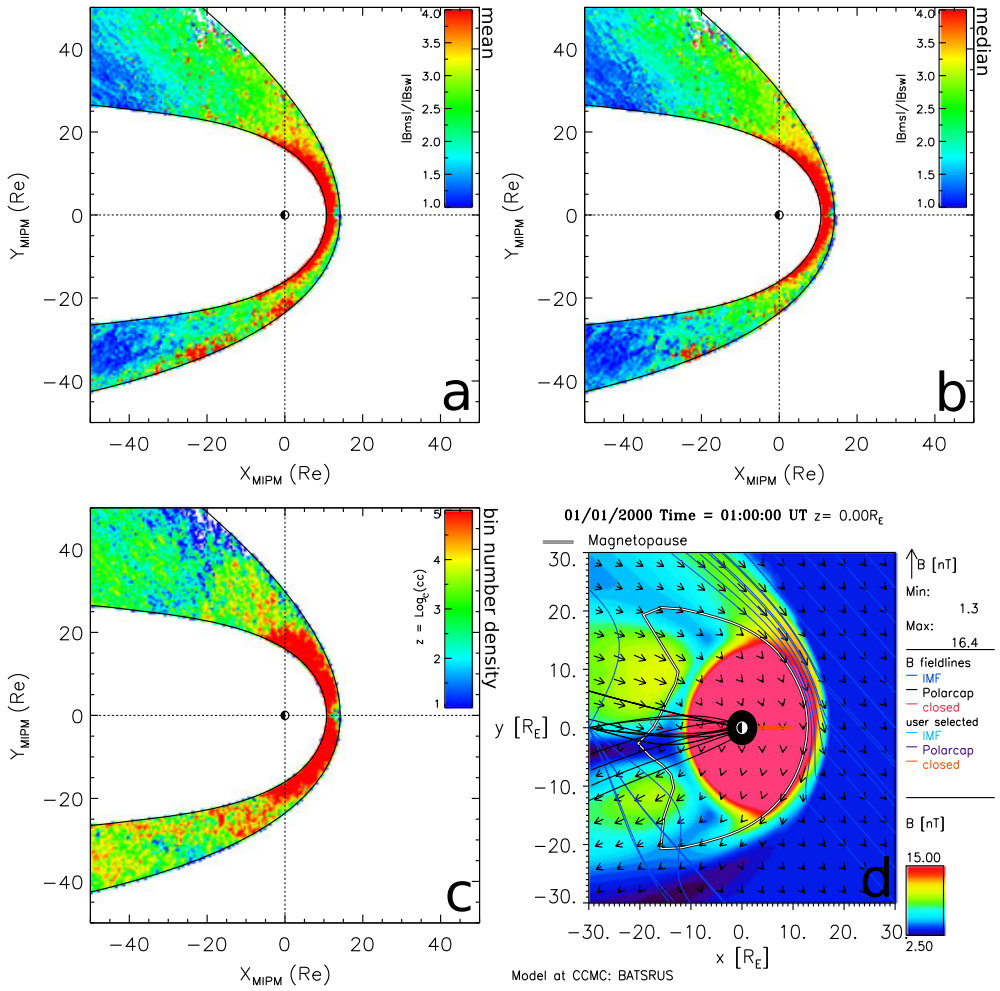

Figure 6. Statistical maps for normalized magnetic field magnitude for all experiment data using the (a) mean and (b) median averages of data, which falls into each 0.5 × 0.5 Re bin. (c) The count per bin (cc) and (d) the MHD simulated result for MS magnetic field magnitude in nT during a PS IMF orientation.

magnetic field profile outlined above. In addition to this, they both indicate stronger magnetic field strengths present on the $\Theta_{\perp}$ flank around the terminator. In support of this observation, Figure 6c demonstrates that there is adequate data coverage in this area. It should also be noted that there are some discrepancies between the mean and median averaged data which can be seen on the $\Theta_{\parallel}$ flank close to the BS around he terminator and downstream. Since these appear sensitive to the mean and median average techniques, then these are likely to be statistical but do not affect our results. There are also enhancements around $X_{mipm} \approx -20$, which seem to manifest in both mean and median averaged data sets.

6. Discussion

[29] The work described in this manuscript has several objectives. (1) From a technical standpoint, we wished to address the problem of boundary motion with regards to presenting large statistical data sets of the MS. (2) The methodology would be used to produce statistical maps of various MS plasma parameters which could be compiled for specific upstream conditions. (3) The statistical data was to be used to investigate the presence of asymmetries of magnetic field, density, and velocity, which had been previously reported.

[30] Objective (1) was approached by the application of the MIPM reference frame [see *Paularena et al.*, 2001; *Němeček et al.*, 2003; *Longmore et al.*, 2005; *Verigin et al.*, 2006] where variations in the MS thickness are addressed by representing data points using the fractional distance across the MS calculated by MP and BS models by *Shue et al.* [1998] and *Verigin et al.* [2001], respectively. Data expressed in the MIPM frame means that statistical data can be compiled under the assumption that MS boundaries are stationary. Throughout the processing of all statistical data, significant measures were taken to maintain the integrity of the final statistical data sets. This was achieved using strict selection criteria imposed on all data windows prior to their inclusion in our results. Objective (2) was addressed by binning the compiled statistical data into a cartesian grid space, which allowed statistical data to be presented for various upstream conditions. These maps were validated and analyzed by comparison with simulated MS profiles from the CCMC BATS-R-US MHD model. Experimental maps were produced for the magnetic field, density, and velocity to provide means of investigating the asymmetries mentioned in objective (3).

6.1. Plasma Velocity

[31] The purpose of Figure 3 is, first, to demonstrate the arrangement of data points in the MIPM and GSE frames and, second, to provide a means of validation for data point placement. The conclusions which should be drawn from these plots are, first, the obvious MIPM dependence on BS geometry controlled by the IMF vector, and second, the confidence in the accuracy of the statistical data.

[32] Presented in Figure 4 was the MS velocity profile based on experimental data and MHD theory. The plots based on our statistical data (Figures 4a and 4b) show faster MS flow velocities on the $\Theta_{\perp}$ flank particularly in the region close to the terminator. Both of the statistical data based on mean and median averaged bins show good agreement with this result. As these statistical data are binned predominantly under a PS IMF, we also compiled OPS data (not shown), but these maps showed little to no clear indication of this asymmetry. There are possible reasons for this however, first, existing studies [*Longmore et al.*, 2005; *Walsh et al.*, 2012] that also observed this asymmetry were not able to find any strict relationship to IMF. Second, there is significantly less statistical data for the OPS case, which results in less global and local (data per bin) data coverage which could easily skew these results. Finally, as cases of OPS are typically shorter in duration, then the statistics of these events may be sporadic, which could suggest that certain features do not have ample time to manifest in these results. Arguably, a more quantitative based technique would be more applicable to this investigation based on extended periods of OPS IMF conditions. However, since MHD theory predicts a symmetric velocity profile, the driving mechanism of the observed asymmetry during PS IMF is likely to be associated with kinetic processes. To eliminate the possibility that these profiles were due to a numerical/processing effect, we compiled data under various averaging times, grid dimensions, and selection criteria, and all maps agreed with the ones presented here. Figure 4c also suggests that there is adequate data coverage within this region. Therefore, since the IMF is typically aligned with the PS geometry, then an obvious conclusion is that the described asymmetry is a predominant feature of the MS velocity profile.

6.2. Proton Density

[33] Previous experimental studies [*Paularena et al.*, 2001; *Longmore et al.*, 2005; *Walsh et al.*, 2012] have demonstrated that larger proton densities are typically located on the dawn flank of the MS by magnitudes of approximately 20%–25%. These studies also concluded that the IMF cannot be the lone cause and in fact may not be the controlling factor at all, especially during periods of solar maximum. As a result, other mechanisms have been proposed which include increased foreshock activity present on the $\Theta_{\parallel}$ flank, the role of upstream plasma waves, and the validity of γ across different Θ_{bn}. In spite of this, the true cause of this asymmetry remains somewhat unsolved. Our results for proton density are presented in Figure 5 which are based on THEMIS observations collected between August 2007 and April 2013. Both the experimental and simulated results show a band of increased density immediately behind the BS nose which corresponds to the region where the MS plasma experiences the greatest compression. This "band" eventually diminishes at $\approx$ 5 Re and then steadily decreases moving along the tailward direction. The agreement between the experimental and MHD results are apparent. Interestingly, in the simulated environment, there appears to be a small asymmetry favoring the dawn flank which conforms to the previously mentioned experimental studies. However, our statistical results do not show clear evidence of this asymmetry. Data binned for other IMF orientations also showed no signs of favoring a specific flank. A possible explanation for the lack of observed asymmetry is that the magnitude is not distinguishable on our color scale, and such a delicate investigation is better suited to quantitative studies. In addition to this, *Paularena et al.* [2001] concluded from their results that stronger density measurements were present during periods of solar maximum. Since the interval of data used to complete this study (2007–2013) corresponds to a transient period from solar minimum (2007) to solar maximum (2013), this asymmetry may not be observable. To investigate this, we compiled statistics for the separate intervals of 2007 to 2010 and then from 2010 to 2012, but the orbital coverage during these times were not sufficient to draw any reliable conclusions. Despite that, with the increasing availability of data during solar maximum, it may be possible to investigate this in the future. Furthermore, the exclusion of any obvious asymmetry in our results is consistent with previous studies such that any density asymmetry could be present but is likely to be on a comparable or lesser extent than has been reported.

6.3. Magnetic Field Strength

[34] The normalized magnetic field profile of the MS compiled from the theoretical and experiential data is presented in Figure 6. A clear result is the strong agreement between our statistical results and those obtained from MHD. First, both the simulated and experimental results show a remarkably similar MS magnetic field profile and, second, the average steady state magnetic field strength appears to be visibly larger on the $\Theta_{\perp}$ flank during PS IMF conditions. This observation is most noticeable on the $\Theta_{\perp}$ flank in the region enclosed between 0 to 5 Re and is present in both the mean and median plots. Although MHD theory predicts this asymmetry, there has also been experimental results which have reached this conclusion. *Walsh et al.* [2012] used THEMIS data to investigate asymmetries of plasma properties close to the MP. In their statistical data, the most prolific difference in the dawn/dusk magnetic field occurred around 3 to 4 h from noon. Although these data were collected in close proximity to the MP, our results tend to agree with their conclusions. *Němeček et al.* [2003] also performed a statistical study of the normalized magnetic field profile and reported a much more dynamic MS on the dayside in comparison to the nightside, which is also supported by our results. There is strong agreement between the magnetic field profiles predicted from the MHD theory and our experimental results. Such similarities suggest that MHD theory performs reasonably well in estimating the general magnetic field profile of the MS. Having said that, waves observed in the MS (e.g., mirror mode waves) [*Verigin et al.*, 2006; *Génot et al.*, 2009; *Balikhin et al.*, 2009; *Balikhin et al.*, 2010] are kinetic by design and have been shown to influence magnetic field. As a result of this, kinetic processes are likely to play some role in the

formation of the MS magnetic field profile and cannot be ignored. It is worth noting that in addition to Figure 6, we compiled magnetic field separately for PS and OPS IMF and, in these data, stronger magnetic fields also favored the $\Theta_{\perp}$ flank. Since both the statistical and theoretical results for PS and OPS data agree that the magnetic field strength is typically stronger on the more compressed $\Theta_{\perp}$ flank, then there is strong evidence that the IMF plays a key role in the MS magnetic field asymmetry. The magnetic field enhancements on the $\Theta_{\parallel}$ flank close to $X_{\mathrm{mipm}} \approx -20$ Re manifest in both averaged data sets and interestingly are a deviation from MHD. These local enhancements could be attributed to kinetic processes, however, the mechanism responsible is currently unclear.

[35] The present paper has demonstrated the statistical mapping of MS velocity, magnetic field and density using THEMIS measurements. The MIPM frame has been used to overcome difficulties associated with the motion of the MS boundaries induced by variations in upstream SW conditions. Throughout the processing of experimental data, we have made rigorous attempts to minimize any induced error introduced at various stages. The greatest opportunity for error in this case is the inaccuracy of the boundary models. To combat this, we have implemented various check conditions to eliminate SW points from our results. A strict selection criteria is also enforced to ensure reliability of our statistical data. Results were also repeated for SW averages of 30 min, and MS averages of 5 min and this did not change our results. The described work presents a flexible methodology which can be used to investigate the MS profile of various derived and measured plasma properties. In addition to this, multiple statistical data can be compiled based on many variations of upstream conditions. The efforts to retain the integrity of our data and the favorable agreement between our results, MHD, and previous studies suggests that there is sufficient accuracy in these results to draw reliable conclusions.

7. Conclusions and Summary

[36] This paper has addressed one of the main difficulties associated with statistical studies of the MS, which is accounting for the significant variations in the MP and BS due to variations in the SW. The present work has addressed this problem by converting THEMIS data which is initially in the GSE frame, to the more robust MIPM frame. The MIPM frame uses boundary models to represent data in terms of the fractional distance across the model MS. We used THEMIS measurements collected between 2007 and 2013 and converted each probe location in the MS to the MIPM frame which forms our statistical data. The OMNI database is used as a means of evaluating the boundary models and also provides the capability of prefiltering the statistical data. The latter permits multiple statistical data to be compiled based on various upstream conditions such as IMF orientation and SW plasma parameters. The statistical data sets are then binned onto a cartesian grid-space with individual bin dimensions of 0.5 × 0.5 Re. The end results from this process are statistical maps of magnetic field strength, density, and MS velocity. Our results show asymmetry of magnetic field and velocity favoring the region of the MS associated with a quasi-perpendicular BS, which agrees with both existing experimental and theoretical studies. Interestingly, the statistical data compiled for density shows no conclusive evidence of asymmetry. Nevertheless, the overall agreement between the experimental MS profiles and the simulated results are apparent for each binned quantity. Discrepancies between MHD theory and our experiential results exist, but this is expected due to the presence of kinetic physics. The velocity asymmetry showed no IMF dependence which strongly suggests that other mechanism must be responsible. In contrast to this, stronger magnetic field strength appeared to favor the $\Theta_{\perp}$ region, which implies that the IMF orientation plays a role in forming the MS magnetic field profile.

[37] To summarize, the main outcome from this work is the application of the MIPM frame to the creation of statistical maps of MS plasma properties used to investigate the presence of asymmetries for magnetic field, density, and velocity. Presented work has shown strong evidence for asymmetry of magnetic field and velocity but not density. The methodology has the flexibility and framework for further development with the inclusion of improved boundary models and the inclusion of additional data sources. The described methodology will facilitate further study of other derived and measured quantities using more sophisticated upstream filtering to closely investigate the dependence of MS plasma properties on upstream conditions. All the conclusions originating from our statistical data are in good agreement with previous experimental studies performed by *Petrinec et al.* [1997], *Paularena et al.* [2001], *Němeček et al.* [2003], *Longmore et al.* [2005], & *Walsh et al.* [2012]. Our results were validated by comparing our statistical data with runs from the BATS-R-US MHD model where the general profile of each parameter showed very strong agreement.

Appendix A: Bow Shock Model Solution

[38] The geocentric distance to the bow shock is calculated from the solution of the following equation:

$$\begin{aligned} r_{\mathrm{BS}}\cos(\theta) &= r_0 + \Delta + \chi R_s(M_{\mathrm{as}}^2 - 1) \\ &\quad -0.5(1-\chi) r_{\mathrm{BS}}\sin(\theta)\sqrt{(M_{\mathrm{as}}^2 - 1)} \\ &\quad -\chi R_s({M_{\mathrm{as}}}^2 - 1)K \end{aligned} \tag{A1}$$

where,

$$K = \sqrt{1 - \frac{(1-\chi) r_{\mathrm{BS}}\sin(\theta)}{\chi R_s\sqrt{M_{\mathrm{as}}^2 - 1}} + \frac{(1+\chi)^2 r_{\mathrm{BS}}^2\sin^2(\theta)}{4\chi^2 R_s^2 (M_{\mathrm{as}}^2 - 1)}} \tag{A2}$$

and,

$$\Delta = R_0 b^{-2/5}\left(\frac{b\epsilon'}{1.87 + 0.86/(b\epsilon')^{3/5}}\right)^{2/3} \tag{A3}$$

and

$$b = 1 - \cos^2(\theta_{bv})/\epsilon M_a^2 \tag{A4}$$

$$\epsilon = \rho_1/\rho_2 \tag{A5}$$

$$\epsilon' = \epsilon/(1-\epsilon) \tag{A6}$$

$$R_s = R_0 b^{-3/4}\left(\frac{1.058 + b\epsilon'}{1.067}\right)^{5/3} \tag{A7}$$

$$\chi = \frac{3.2}{M_{\mathrm{as}} + 1} \tag{A8}$$

In the above expressions, R_s and χ are both shaping parameters. $\rho_{1,2}$ are the upstream and downstream plasma densities, respectively. The downstream density at the bow shock nose is not known; therefore, the Rankine-Hugoniot relation is used to calculate this value [*Zhuang and Russell*, 1981; *Verigin et al.*, 2001].

$$\epsilon^3 - \left(\frac{A}{B} + \frac{A+1+(B+2)C}{BM_a{}^2} + \frac{2}{BM_s{}^2}\right)\epsilon^2 - \frac{C}{BM_a{}^4}\left(A + \frac{2C}{M_s{}^2}\right)\epsilon + \frac{1}{BM_a{}^2}(A+1\left(1+C) + C\left(\frac{B}{M_a{}^2} + \frac{4}{M_a{}^2}\right)\right) = 0 \tag{A9}$$

where $A = \gamma - 1$ and $B = \gamma + 1$ and $C = \cos^2\theta_{\mathrm{bv}}$. The variable γ is the ratio of specific heats of the solar wind, in this study it is assumed to be 5/3.

[39] The calculation of the parameter M_{as} is more involved as it requires the exact MHD solution of the asymptotic Mach cone angle ω.

$$M_{\mathrm{as}} = \frac{1}{\sin(\omega)} \tag{A10}$$

A1. The Mach Cone Angle Solution

[40] The solution of the Mach cone angle requires the trivial solution of the following expression for the parameter ω. [*Verigin et al.*, 2003]

$$\tan(\omega) = \frac{1}{a} \tag{A11}$$

However, this requires the computation of three additional parameters a, b, and c

$$a(b, c, \phi) = -b\cos(\phi) + c\sin(\phi) \tag{A12}$$

C is determined from the solution of the following equation

$$c = \tan(\phi)\left(\frac{M_a^2 M_s^2}{\left(M_a^2 + M_s^2 - \left(b\sin(\theta_{\mathrm{bv}}) + \cos(\theta_{\mathrm{bv}})\right)^2\right)^2} - b\right) \tag{A13}$$

and b requires the solution of the following 10th-order polynomial

$$\tan^2(\phi)\left(\frac{M_a^2 M_s^2 (b\sin(\theta_{bv}) + \cos(\theta_{bv}))\sin(\theta_{bv})}{1} - b\right)^2 = \frac{M_a^2 M_s^2}{M_a^2 + M_s^2 - (b\sin(\theta_{bv}) + \cos(\theta_{bv}))^2} - b^2 - 1 \tag{A14}$$

The angle θ_{bv} is the angle between the $\mathbf{V}_u$ and $\mathbf{B}_u$. There are several solutions to equation (A14), which correspond to the fast and slow MHD shock modes. For the terrestrial bow shock, we are only interested in the fast mode solution. The roots all lie between the asymptotes determined by

$$b = \frac{-\cos\theta_{\mathrm{bv}} \pm \sqrt{M_a{}^2 + M_s{}^2}}{\theta_{\mathrm{bv}}} \tag{A15}$$

[41] **Acknowledgments.** The work by A. Dimmock and K. Nykyri was supported by NSF grant 0847120. The OMNI data were obtained from the GSFC/SPDF OMNIWeb interface at http://omniweb.gsfc.nasa.gov. Simulation results have been provided by the Community Coordinated Modeling Center at Goddard Space Flight Center through their public Runs on Request system (http://ccmc.gsfc.nasa.gov). The CCMC is a multiagency partnership between NASA, AFMC, AFOSR, AFRL, AFWA, NOAA, NSF, and ONR. The BATS-R-US Model was developed by the Computational Magnetohydrodynamics (MHD) Group at the University of Michigan, now Center for Space Environment Modeling (CSEM).

[42] Philippa Browning thanks the reviewers for their assistance in evaluating this paper.

References

Acuña, M. H., K. W. Ogilvie, D. N. Baker, S. A. Curtis, D. H. Fairfield, and W. H. Mish (1995), The global geospace science program and its investigations, *Space Sci. Rev.*, *71*, 5–21, doi:10.1007/BF00751323.

Angelopoulos, V. (2008), The THEMIS mission, *Space Sci. Rev.*, *141*, 5–34, doi:10.1007/s11214-008-9336-1.

Auster, H. U., et al. (2008), The THEMIS fluxgate magnetometer, *Space Sci. Rev.*, *141*, 235–264, doi:10.1007/s11214-008-9365-9.

Balikhin, M., V. Krasnosselskikh, and M. Gedalin (1995), The scales in quasiperpendicular shocks, *Adv. Space Res.*, *15*, 247–260, doi:10.1016/0273-1177(94)00105-A.

Balikhin, M. A., R. Z. Sagdeev, S. N. Walker, O. A. Pokhotelov, D. G. Sibeck, N. Beloff, and G. Dudnikova (2009), THEMIS observations of mirror structures: Magnetic holes and instability threshold, *Geophys. Res. Lett.*, *36*, L03105, doi:10.1029/2008GL036923.

Balikhin, M. A., O. A. Pokhotelov, S. N. Walker, R. J. Boynton, and N. Beloff (2010), Mirror mode peaks: THEMIS observations versus theories, *Geophys. Res. Lett.*, *37*, L05104, doi:10.1029/2009GL042090.

Bieber, J. W., and S. C. Stone (1979), Energetic electron bursts in the magnetopause electron layer and in interplanetary space, in *Magnetospheric Boundary Layers*, edited by B. Battrick, J. Mort, and G. Haerendel, *Eur. Space Agency Spec. Publ., ESA SP-148*, 131–135.

Dimmock, A. P., M. A. Balikhin, V. V. Krasnoselskikh, S. N. Walker, S. D. Bale, and Y. Hobara (2012), A statistical study of the cross-shock electric potential at low Mach number, quasi-perpendicular bow shock crossings using Cluster data, *J. Geophys. Res.*, *117*, 2210, doi:10.1029/2011JA017089.

Farris, M. H., and C. T. Russell (1994), Determining the standoff distance of the bow shock: Mach number dependence and use of models, *J. Geophys. Res.*, *99*(17), 681, doi:10.1029/94JA01020.

Formisano, V. (1979), Orientation and shape of the Earth's bow shock in three dimensions, *Planet. Space Sci.*, *27*, 1151–1161, doi:10.1016/0032-0633(79)90135-1.

Frey, S., V. Angelopoulos, M. Bester, J. Bonnell, T. Phan, and D. Rummel (2008), Orbit design for the THEMIS mission, *Space Sci. Rev.*, *141*, 61–89, doi:10.1007/s11214-008-9441-1.

Génot, V., E. Budnik, P. Hellinger, T. Passot, G. Belmont, P. M. Trávníček, P.-L. Sulem, E. Lucek, and I. Dandouras (2009), Mirror structures above and below the linear instability threshold: Cluster observations, fluid model and hybrid simulations, *Ann. Geophys*, *27*, 601–615, doi:10.5194/angeo-27-601-2009.

Hietala, H., N. Partamies, T. V. Laitinen, L. B. N. Clausen, G. Facskó, A. Vaivads, H. E. J. Koskinen, I. Dandouras, H. Rème, and E. A. Lucek (2012), Supermagnetosonic subsolar magnetosheath jets and their effects: From the solar wind to the ionospheric convection, *Ann. Geophys.*, *30*, 33–48, doi:10.5194/angeo-30-33-2012.

Hobara, Y., M. Balikhin, V. Krasnoselskikh, M. Gedalin, and H. Yamagishi (2010), Statistical study of the quasi-perpendicular shock ramp widths, *J. Geophys. Res.*, *115*(11), 106, doi:10.1029/2010JA015659.

King, J. H., and N. E. Papitashvili (2005), Solar wind spatial scales in and comparisons of hourly Wind and ACE plasma and magnetic field data, *J. Geophys. Res.*, *110*, A02104, doi:10.1029/2004JA010649.

Lavraud, B., J. E. Borovsky, A. J. Ridley, E. W. Pogue, M. F. Thomsen, H. Rème, A. N. Fazakerley, and E. A. Lucek (2007), Strong bulk plasma acceleration in Earth's magnetosheath: A magnetic slingshot effect? *Geophys. Res. Lett.*, *34*, L14102, doi:10.1029/2007GL030024.

Lavraud, B., et al. (2013), Asymmetry of magnetosheath flows and magnetopause shape during low Alfvén Mach number solar wind, *J. Geophys. Res. Space Phys.*, 1–12, doi:10.1002/jgra.50145.

Longmore, M., S. J. Schwartz, J. Geach, B. M. A. Cooling, I. Dandouras, E. A. Lucek, and A. N. Fazakerley (2005), Dawn-dusk asymmetries and sub-Alfvénic flow in the high and low latitude magnetosheath, *Ann. Geophys.*, *23*, 3351–3364, doi:10.5194/angeo-23-3351-2005.

McFadden, J. P., C. W. Carlson, D. Larson, M. Ludlam, R. Abiad, B. Elliott, P. Turin, M. Marckwordt, and V. Angelopoulos (2008), The THEMIS ESA plasma instrument and in-flight calibration, *Space Sci. Rev.*, *141*, 277–302, doi:10.1007/s11214-008-9440-2.

Newbury, J. A., and C. T. Russell (1996), Observations of a very thin collisionless shock, *Geophys. Res. Lett.*, *23*, 781–784, doi:10.1029/96GL00700.

Němeček, Z., J. Šafránková, G. N. Zastenker, P. Pišoft, K. I. Paularena, and J. D. Richardson (2000), Observations of the radial magnetosheath profile and a comparison with gasdynamic model predictions, *Geophys. Res. Lett.*, *27*, 2801–2804, doi:10.1029/2000GL000063.

Němeček, Z., M. Hayosh, J. Šafránková, G. N. Zastenker, and J. D. Richardson (2003), The dawn-dusk asymmetry of the magnetosheath: INTERBALL-1 observations, *Adv. Space Res.*, *31*, 1333–1340, doi:10.1016/S0273-1177(03)00007-3.

Papadopoulos, K. (1985), Microinstabilities and anomalous transport, *Washington DC Am Geophys. Union (Geophysical Monograph Series)*, *34*, 59–90.

Paularena, K. I., J. D. Richardson, M. A. Kolpak, C. R. Jackson, and G. L. Siscoe (2001), A dawn-dusk density asymmetry in Earth's magnetosheath, *J. Geophys. Res.*, *106*, 25,377–25,394., doi:10.1029/2000JA000177.

Peredo, M., J. A. Slavin, E. Mazur, and S. A. Curtis (1995), Three-dimensional position and shape of the bow shock and their variation with Alfvénic, sonic and magnetosonic Mach numbers and interplanetary magnetic field orientation, *J. Geophys. Res.*, *100*, 7907–7916, doi:10.1029/94JA02545.

Petrinec, S. M., T. Mukai, A. Nishida, T. Yamamoto, T. K. Nakamura, and S. Kokubun (1997), Geotail observations of magnetosheath flow near the magnetopause, using Wind as a solar wind monitor, *J. Geophys. Res.*, *102*, 26,943–26,960, doi:10.1029/97JA01637.

Sagdeev, R. Z. (1966), Cooperative phenomena and shock waves in collisionless plasmas, *Rev. Plasma Phys.*, *4*, 23–90.

Sagdeev, R. Z., and A. A. Galeev (1969), *Nonlinear Plasma Theory*, W.A. Benjamin, New York.

Shue, J. -H., et al. (1998), Magnetopause location under extreme solar wind conditions, *J. Geophys. Res.*, *103*, 17,691–17,700, doi:10.1029/98JA01103.

Stone, E. C., A. M. Frandsen, R. A. Mewaldt, E. R. Christian, D. Margolies, J. F. Ormes, and F. Snow (1998), The advanced composition explorer, *Space Sci. Rev.*, *86*, 1–22, doi:10.1023/A:1005082526237.

Tóth, G., et al. (2005), Space weather modeling framework: A new tool for the space science community, *J. Geophys. Res.*, *110*, A12226, doi:10.1029/2005JA011126.

Verigin, M., J. Slavin, A. Szabo, G. Kotova, and T. Gombosi (2003), Planetary bow shocks: Asymptotic MHD Mach cones, *Earth, Planets, Space*, *55*, 33–38.

Verigin, M. I., et al. (2001), Analysis of the 3-D shape of the terrestrial bow shock by interball/magion 4 observations, *Adv. Space Res*, *28*, 857–862, doi:10.1016/S0273-1177(01)00502-6.

Verigin, M. I., M. Tátrallyay, G. Erdős, and G. A. Kotova (2006), Magnetosheath interplanetary medium reference frame: Application for a statistical study of mirror type waves in the terrestrial plasma environment, *Adv. Space Res.*, *37*, 515–521, doi:10.1016/j.asr.2005.03.042.

Walsh, B. M., D. G. Sibeck, Y. Wang, and D. H. Fairfield (2012), Dawn-dusk asymmetries in the Earth's magnetosheath, *J. Geophys. Res. Space Phys.*, *117*, A12, doi:10.1029/2012JA018240.

Wing, S., J. R. Johnson, P. T. Newell, and C.-I. Meng (2005), Dawn-dusk asymmetries, ion spectra, and sources in the northward interplanetary magnetic field plasma sheet, *J. Geophys, Res.*, *110*, A08205, doi:10.1029/2005JA011086.

Zhuang, H. C., and C. T. Russell (1981), An analytic treatment of the structure of the bow shock and magnetosheath, *J. Geophys. Res.*, *86*, 2191–2205, doi:10.1029/JA086iA04p02191.